AGU100 ADVANCING EARTH AND SPACE SCIENCE

Geophysical Research Letters

16 January 2019 · Volume 46 · Issue 1

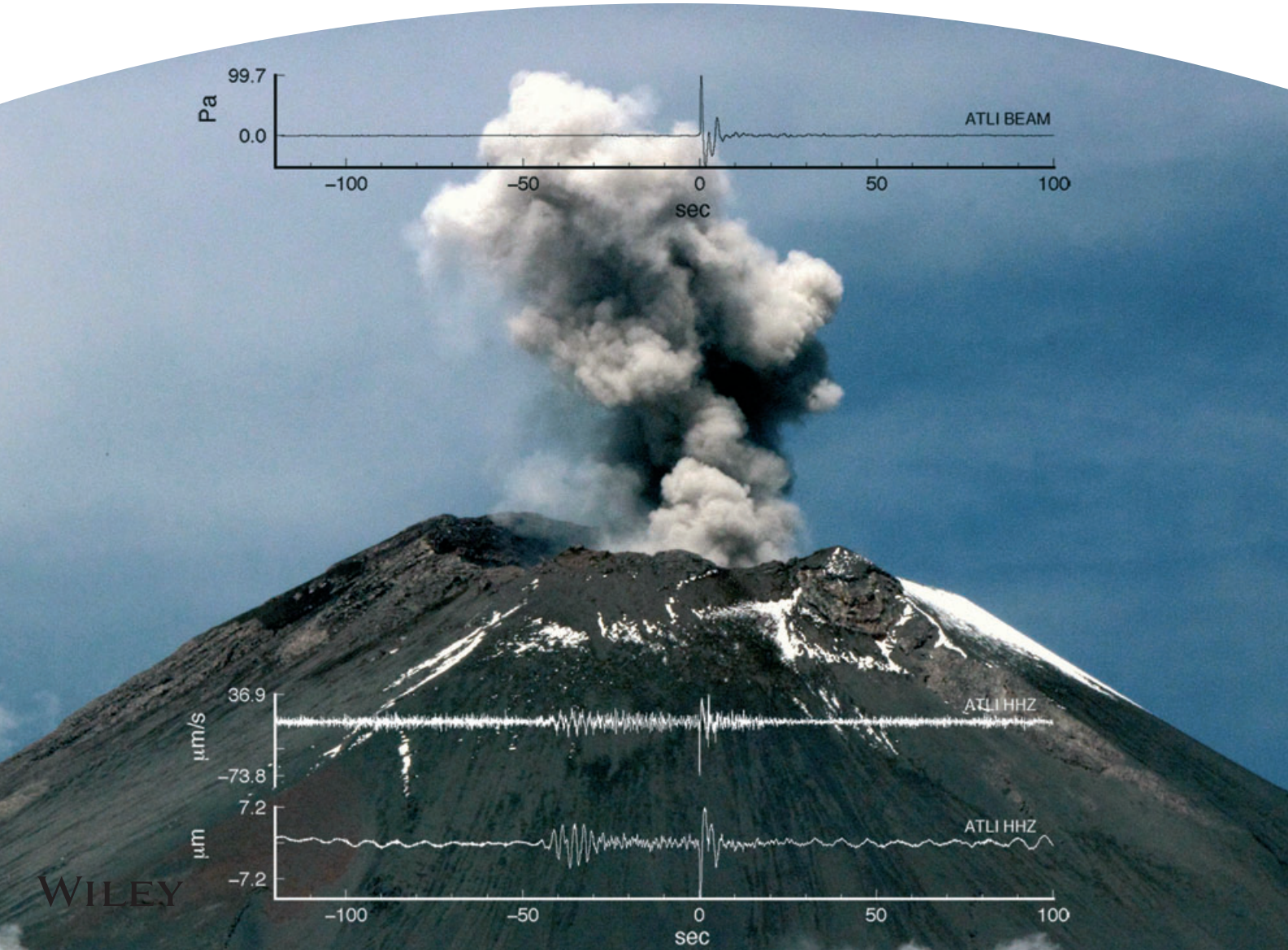

WILEY

Geophysical Research Letters

AN AGU JOURNAL

Aims and Scope. *Geophysical Research Letters* publishes high-impact, innovative, and timely research on major scientific advances in all the major geoscience disciplines. Papers are communications-length articles and should have broad and immediate implications in their discipline or across the geosciences. GRL maintains the fastest turn-around of all high-impact publications in the geosciences and works closely with authors to ensure broad visibility of top papers.

AGU Editorial Team. For assistance with submitted manuscripts, file specifications, or AGU publication policy please contact grlonline@agu.org.

For submission instructions or to submit a manuscript visit: http://grl-submit.agu.org.

The journal to which you are submitting your manuscript employs a plagiarism detection system. By submitting your manuscript to this journal you accept that your manuscript may be screened for plagiarism against previously published works.

Geophysical Research Letters accepts articles for Open Access publication. Please visit http://olabout.wiley.com/WileyCDA/Section/id-406241.html for further information about OnlineOpen.

Publication Charges. The publication charge income received for *Geophysical Research Letters* helps support rapid publication, allows more articles per volume, makes possible the low subscription rates, and supports many of AGU's scientific and outreach activities. Publication charge information can be found here: http://publications.agu.org/author-resource-center/.

To encourage papers to be written in a concise fashion, there is an excess length fee. For *Geophysical Research Letters* the fee is assessed only on the equivalent of more than 12 publication units. The excess length fee does not apply to review articles, and the editor may waive the fee on a limited number of concisely written papers that merit being longer. There is no charge for color in any format.

Individual Subscriptions. Member subscriptions are available through members.agu.org or by contacting the AGU Member Service Center. The Service Center is open from 8:00 a.m. to 8:30 p.m. Eastern time: +1 202 462 6900, +1 800 966 2481; Fax: +1 202 777 7393; e-mail: service@agu.org. Questions about meetings or membership will be referred to the appropriate staff.

Publisher. *Geophysical Research Letters* is published on behalf of the American Geophysical Union by Wiley Periodicals, Inc., 111 River St., Hoboken, NJ, 07030-5774, +1 201 748 6000.

Delivery Terms and Legal Title. Where the subscription price includes print issues and delivery is to the recipient's address, delivery terms are Delivered at Place (DAP); the recipient is responsible for paying any import duty or taxes. Title to all issues transfers FOB our shipping point, freight prepaid. We will endeavour to fulfil claims for missing or damaged copies within six months of publication, within our reasonable discretion and subject to availability.

GEOPHYSICAL RESEARCH LETTERS, (ISSN 0094-8276), is published semi-monthly by Wiley Subscription Services, Inc., a Wiley Company, 111 River St., Hoboken, NJ 07030-5774.

Periodical Postage Paid at Hoboken, NJ and additional offices.

Postmaster: Send all address changes to GEOPHYSICAL RESEARCH LETTERS, John Wiley & Sons Inc., C/O The Sheridan Press, PO Box 465, Hanover, PA 17331.

Journal Customer Services. For institutional subscription information, claims and any enquiry concerning your journal subscription please go to www.wileycustomerhelp.com/ask or contact your nearest office.

Americas: Email: cs-journals@wiley.com; Tel: +1 781 388 8598 or +1 800 835 6770 (toll free in the USA & Canada).
Europe, Middle East and Africa: Email: cs-journals@wiley.com; Tel: +44 (0) 1865 778315.
Asia Pacific: Email: cs-journals@wiley.com; Tel: +65 6511 8000.
Japan: For Japanese speaking support, Email: cs-japan@wiley.com; Tel: +65 6511 8010 or Tel (toll-free): 005 316 50 480.

Visit our Online Customer Help available in 7 languages at www.wileycustomerhelp.com/ask.

Production Editor. For assistance with post-acceptance articles and other production issues please contact GRLprod@wiley.com.

Access to this journal is available free online within institutions in the developing world through the AGORA initiative with the FAO, the HINARI initiative with the WHO, the OARE initiative with UNEP, and the ARDI initiative with WIPO. For information, visit www.aginternetwork.org, www.who.int/hinari/en/, www.oaresciences.org, or www.wipo.int/ardi/en.

ISSN 0094-8276 (Print)
ISSN 1944-8007 (Online)

View this journal online at http://grl.agu.org

Cover: Seismo-acoustic signature of a Vulcanian explosion at Popocatépetl volcano, Mexico. Waveforms from a four-element broadband infrasound array colocated with a compact broadband seismometer at a site 15.8 km to the east-southeast of Popocatépetl's summit. The infrasound waveforms (top) are highly asymmetric and are associated with clear air-ground coupled arrivals on seismometers (bottom), with inverted vertical displacement waveforms tracking infrasonic pressure waveforms. Popocatépetl is a highly active andesitic stratovolcano with regular violent explosions; this project is investigating the capability of infrasound stations at distances greater than 5 km to monitor Popocatépetl with significantly reduced risk exposure to field personnel and instrumentation. See also Matoza et al. (pp. 148–157; https://doi.org/10.1029/2018GL080802). Image credit: Alejandro Rosado-Fuentes.

AGU100 ADVANCING EARTH AND SPACE SCIENCE

Geophysical Research Letters

RESEARCH LETTER
10.1029/2018GL080802

Key Points:
- Infrasound array study of Popocatépetl; high broadband (200-Hz sample rate) includes sub-bass range
- Vulcanian explosions produce high-amplitude asymmetric infrasound, which is air-ground coupled
- Inverted vertical displacement seismic waveforms track infrasonic pressure waveforms

Supporting Information:
- Supporting Information S1
- Data Set S1

Correspondence to:
R. S. Matoza,
matoza@geol.ucsb.edu

Citation:
Matoza, R. S., Arciniega-Ceballos, A., Sanderson, R. W., Mendo-Pérez, G., Rosado-Fuentes, A., & Chouet, B. A. (2019). High-broadband seismoacoustic signature of Vulcanian explosions at Popocatépetl volcano, Mexico. *Geophysical Research Letters*, *46*, 148–157. https://doi.org/10.1029/2018GL080802

Received 8 OCT 2018
Accepted 18 NOV 2018
Accepted article online 21 NOV 2018
Published online 13 JAN 2019

High-Broadband Seismoacoustic Signature of Vulcanian Explosions at Popocatépetl Volcano, Mexico

Robin S. Matoza[1], Alejandra Arciniega-Ceballos[2], Richard W. Sanderson[1], Gerardo Mendo-Pérez[3], Alejandro Rosado-Fuentes[3], and Bernard A. Chouet[4]

[1]Department of Earth Science and Earth Research Institute, University of California, Santa Barbara, CA, USA, [2]Departamento de Vulcanología, Instituto de Geofísica, Universidad Nacional Autónoma de México, México City, Mexico, [3]Posgrado en Ciencias de la Tierra, Instituto de Geofísica, Universidad Nacional Autónoma de México, México City, Mexico, [4]Arzier-Le Muids, Switzerland

Abstract We present high-broadband infrasound (~0.01–100 Hz; 200-Hz sample rate) observations of Vulcanian explosions at Popocatépetl volcano, Mexico. Popocatépetl is a highly active andesitic stratovolcano with regular violent explosions, making it a promising target for seismoacoustic observations. We deployed a four-element broadband infrasound array (aperture ~50 m) colocated with a compact broadband (120 s) seismometer at a site (ATLI) 15.8 km to the east-southeast of Popocatépetl's summit. We highlight waveform examples from five powerful explosions during October to December 2017 that produced infrasound zero-to-peak pressure amplitudes ranging from ~30 to 100 Pa at ATLI. The infrasound waveforms are highly asymmetric and are associated with clear air-ground-coupled arrivals on seismometers, with inverted vertical displacement waveforms tracking infrasonic pressure waveforms. Popocatépetl is close to major population centers, and array processing reveals persistent background infrasound from multiple directions, presumably of anthropogenic origin; our results have implications for infrasound monitoring at populated volcanoes.

Plain Language Summary Seismology and acoustics are complementary methods for quantifying volcanic eruption processes, corresponding to elastic wavefields propagating through the solid Earth and acoustic wavefields propagating through the fluid atmosphere, respectively. Seismic data currently form the backbone of most volcano-monitoring systems. Seismic signals at erupting volcanoes capture subsurface magma transport and rapid depressurization associated with explosive eruptions. Infrasound (acoustic waves with frequencies below 20 Hz, the lower-frequency limit of human hearing) is a newer technology; infrasound data record subaerial degassing and allow physical quantification of explosive eruption mechanisms. Popocatépetl is one of the two most active volcanoes in Mexico (together with Volcán de Colima) and a prodigious source of explosive activity, making it an obvious target for combined seismic and infrasound (seismoacoustic) observations. We recorded continuous infrasound and seismic waveform data at a site 15.8 km to the east-southeast of Popocatépetl for several months, capturing five powerful explosions. Our data were collected at a location where local people report hearing sounds associated with visual observations of explosions from Popocatépetl. Part of the motivation of this work is to investigate the capability of infrasound stations at distances greater than 5 km to monitor Popocatépetl with significantly reduced risk exposure to field personnel and instrumentation.

1. Introduction

Popocatépetl (19.023°N, 98.622°W; *smoking mountain* in Náhuatl language) is an active 5,452-m-high andesitic stratovolcano located in the central region of the Trans-Mexican Volcanic Belt (Figure 1); it is the second highest mountain and one of the two most active volcanoes in Mexico (together with Volcán de Colima). Popocatépetl is close to major population centers such as Puebla City (45 km) and Mexico City (60 km); millions of people and infrastructure are exposed to risk from its eruptions (De la Cruz-Reyna & Siebe, 1997; Martin Del Pozzo et al., 2017). During the past 5,000 years, major Plinian eruptions from Popocatépetl have occurred at least 4 to 5 times, impacting the environment of the entire region, with the effects on human settlements and agriculture imprinted in the archeologic and geologic records (Panfil et al., 1999; Siebe et al., 1995, 1996,

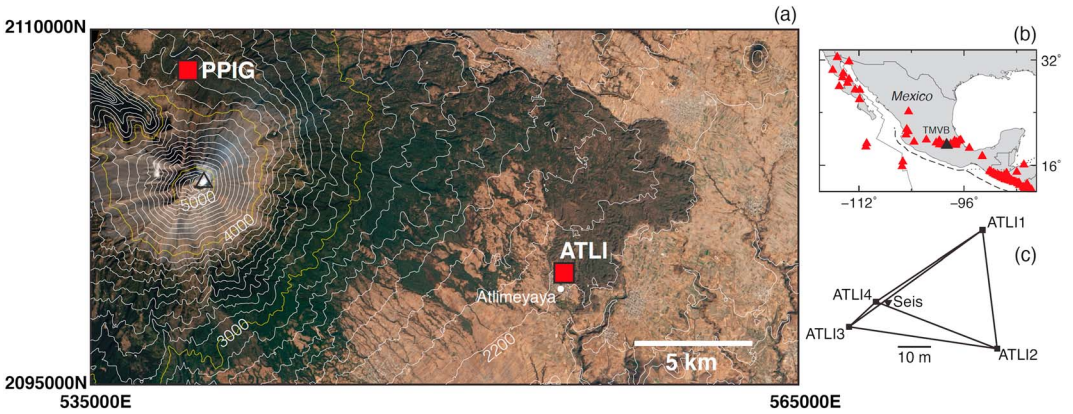

Figure 1. (a) Map showing the location of the ATLI station (high-broadband infrasound array and seismometer) and broadband seismic station PPIG in UTM zone 14°N coordinates. Contour interval is 100 m in elevation from Advanced Spaceborne Thermal Emission and Reflection Radiometer topography; select contours are labeled, with 3,000, 4,000, and 5,000 m contours shown in yellow. The ATLI array is at 2,240-m elevation above sea level. The active vent of Popocatépetl is indicated by a black triangle. The basemap is a 4 January 2011 National Aeronautics and Space Agency Earth Observatory image. (b) Regional map showing potentially active Holocene (past 10,000 years) volcanoes (red triangles; Global Volcanism Program, 2013), tectonic plate boundaries (black lines; Coffin et al., 1998), and national boundaries (black lines). Popocatépetl is shown as a black triangle in the Trans-Mexican Volcanic Belt (TMVB). (c) The ATLI array geometry on equal-scale Cartesian axes; vertical is north. See supporting information (Figure S1) for a regional map showing ATLI and nearby population centers.

1999). Eruptive activity has been comparatively mild during the last few centuries (e.g., De la Cruz-Reyna et al., 2007).

After nearly 70 years of quiescence, Popocatépetl underwent a significant reactivation in December 1994 and since then its eruptive activity has been dominated by hydrothermal processes and magmatic degassing, characterized by periodic emissions of gas and ash, occasional Vulcanian explosions, episodic passive effusions of lava, and the extrusion and destruction of lava domes. All of these eruptive dynamics result in abundant seismicity, including long-period and very-long-period events, tremor, and explosion signals (Arciniega-Ceballos et al., 1999, 2000, 2003, 2008, 2012; Arámbula-Mendoza et al., 2016; Chouet et al., 2005; De la Cruz-Reyna et al., 2008; Roman, 2017). This activity is associated with rumbling and roaring sounds that can commonly be heard in different localities within about 20 km surrounding Popocatépetl (and occasionally farther, e.g., Puebla, ~45 km, presumably for larger explosions and as propagation conditions such as wind direction allow). Since its 1994 reactivation, Popocatépetl has been continuously monitored with seismic, Global Positioning System (GPS), gas, and visual techniques and has become a well-documented case study in volcanology (Delgado-Granados et al., 2008).

Infrasound technology adds to a growing suite of geophysical tools available to characterize, understand, and monitor volcanic processes. Shallow and subaerial volcanic processes radiate infrasound directly into the atmosphere; sampling this infrasound complements seismic data and aids with physical quantification of explosive eruption mechanisms (e.g., Fee & Matoza, 2013; Garcés et al., 2013; Johnson & Ripepe, 2011; Matoza et al., 2019, and references therein). Popocatépetl is an obvious target for infrasonic study, but previous observations have been limited. On 24 February 1664, an explosion at Popocatépetl apparently caused windows and doors in Puebla to burst open (Delgado-Granados et al., 2008, and references therein). Raga et al. (2002) presented long-period and low-sample rate (1 Hz) microbarograph recordings (11.4-km distance) of Popocatépetl explosions, performing numerical simulations of the atmospheric expansion waves using a compressible gas dynamics formulation. Arámbula-Mendoza et al. (2013) describe short-period (flat response 1–5 Hz, limited dynamic range) infrasound recordings at distances of 4.8 and 8.4 km from Popocatépetl. Here we present high broadband (~0.01–100 Hz; 200 Hz sample rate) and high dynamic range infrasound array observations of Popocatépetl explosions, capturing Popocatépetl explosion acoustics with unprecedented fidelity. Infrasound technology has clear potential to augment the existing monitoring systems at Popocatépetl. However, Popocatépetl's activity presents logistical challenges, and part of our motivation is to investigate the capability of arrays at distances greater than 5 km to monitor the volcano with significantly reduced risk exposure to field personnel and instrumentation.

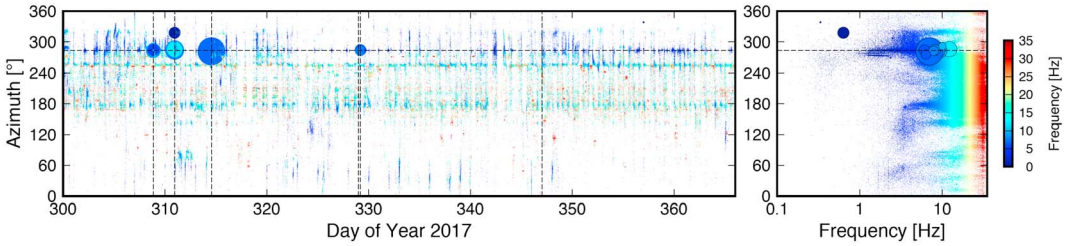

Figure 2. Progressive Multichannel Correlation (PMCC) array processing results for the ATLI array from 27 October to 31 December 2017 (days 300 to 365, 2017); all times in UT. (left panel) Coherent acoustic plane wave arrivals as a function of time are displayed as filled circles at the backazimuth of arrival, with the color scale representing the mean signal frequency and the symbol size proportional to root-mean-square signal amplitude. More than one PMCC detection (filled circle) can be associated with each individual explosion event. The horizontal dashed line indicates the backazimuth to Popocatépetl (283.7°). The vertical dashed lines represent network-coincident STA/LTA detections derived from a separate processing with the infrasound waveforms (see text for details), corresponding to five explosion signal detections at ATLI at times 20:41:22.075 4 November (day 308) 2017; 22:54:28.760 6 November (day 310) 2017; 13:35:35.175 10 November (day 314) 2017; 23:55:47.205 24 November (day 328) 2017; and 04:53:21.470 25 November (day 329) 2017. A sixth STA/LTA trigger on 13 December 2017 (day 347) results from a data glitch. (right panel) As in the left panel but displayed in frequency-azimuth space. There is a spurious large-amplitude detection associated with the day 310 event, which appears at a higher azimuth and lower frequency than the true event from Popocatépetl. We interpret this as a processing artifact resulting from the large-amplitude explosion signal biasing the root-mean-square amplitude calculation for an ambient infrasound signal. STA/LTA = short-term average/long-term average.

2. An Infrasound Array Study of Popocatépetl

In September 2017, we deployed a four-element infrasound array (aperture ~50 m) colocated with a broadband seismometer at a site (ATLI, Atlimeyaya, Puebla) 15.8 km to the east-southeast of Popocatépetl's summit (Figure 1). The array (ATLI) consisted of four broadband Hyperion IFS-3111 infrasound sensors with sensitivity set to record pressures ±500 Pa on scale (1,000 Pa full-scale range) and two channels (vertical and radial) of a 120-s Trillium Compact Posthole seismometer (total number of channels limited by the six-channel digitizer). The continuous waveform data were sampled at 200 Hz and recorded locally on a six-channel 24-bit REF TEK 130S digitizer; all sensors have a flat response from ~0.01 to 100 Hz. The seismometer was directly buried ~1 m deep. The infrasound array element locations were determined with a differential GPS. Each infrasound sensor was equipped with a high-frequency wind shroud for wind-noise reduction and deployed directly outdoors. The ATLI site was chosen considering its orientation with respect to the crater shape; Popocatépetl currently has an asymmetric crater, with shallower crater walls and less topographic blocking to the east and approximately toward the ATLI site (Figure 1). ATLI is in a location where local people report hearing sounds associated with visual observations of emissions, indicating audible acoustic frequencies (>20 Hz) at this distance. We also utilize data from broadband seismic station PPIG 4.9 km from the summit (Figure 1), part of the permanent network monitoring Popocatépetl, and consisting of a Streckeisen STS-2 seismometer with a 24-bit Quanterra Q330 digitizer sampling at 100 Hz deployed in a concrete vault.

We set the sample rate at ATLI to 200 Hz, capturing frequencies up to a Nyquist frequency of 100 Hz. According to the International Federation of Digital Seismograph Networks (FDSN) Standard for the Exchange of Earthquake Data (SEED), the ATLI data are accordingly classified as *high broadband* (band code H), which corresponds to sample rates from ≥80 to <250 Hz combined with instrumentation with a corner period ≥10 s (Ahern & Dost, 2012). We present example signals from Popocatépetl containing frequencies extending up to the Nyquist frequency. Infrasound refers to acoustic waves below 20 Hz, the lower-frequency limit of human hearing. The band from 20 Hz up to 100 Hz is loosely termed the *sub-bass* range. Our high-broadband ATLI data thus capture Popocatépetl acoustic signals in the infrasound and sub-bass ranges.

We operated the ATLI array continuously from 15 September 2017 to 9 June 2018, but encountered logistical challenges and some equipment damage resulting in part from impacts of the nearby M_w 7.1 Puebla (Central Mexico) earthquake, 19 September 2017. Here we focus on a time period from 27 October to 31 December 2017 (days 300 to 365 of 2017, Figure 2), in which all channels of the ATLI array (infrasonic and seismic) were functioning normally.

3. Infrasound Data Processing

3.1. Background Infrasound Sources at Popocatépetl

Infrasound arrays permit the identification of coherent infrasound signals of interest within background incoherent wind noise (Walker & Hedlin, 2010) and unwanted ambient infrasound signals (Garcés et al., 2003; Matoza et al., 2007, 2013). Infrasound array processing also enables discrimination between acoustic and seismic arrivals (e.g., ground-air wave conversion or mechanical shaking of sensors) based on the apparent velocity across the array.

We process the ATLI infrasound array data using the Progressive Multichannel Correlation (PMCC) method (Cansi, 1995; Cansi & Klinger, 1997; Le Pichon et al., 2010). PMCC estimates wavefront parameters (e.g., backazimuth, apparent velocity, root-mean-square amplitude) of coherent plane waves using correlation time-delays between successive array element triplets or subnetworks. PMCC performs a grid search for coherent signals in advancing time windows over a set of frequency bands defined with band-pass filters, forming a pixelated time-frequency representation of coherent infrasound. We use 30 log-spaced frequency bands from 0.01 to 40 Hz with window lengths varying from 200 to 30 s and time steps of 10% of the window length (parameters adapted from Matoza et al., 2013, to extend to the higher frequencies considered here).

The ATLI array records a variety of ambient acoustic signals (Figure 2). The relatively small array aperture (aperture ∼50 m, Figure 1c) results in relatively few array detections of microbaroms (signals from ∼0.1 to 1 Hz) (Landès et al., 2012). These occasional Pacific microbarom detections arrive at a similar backazimuth to those from Popocatépetl (backazimuth from ATLI to Popocatépetl is 283.7°) but can be discriminated from the volcanic signals based on frequency content (Figure 2). Mexico City (distance ∼60 km) also falls at a similar backazimuth to Popocatépetl as viewed from ATLI (∼290–335°; see supporting information, Figure S1), and presumably contributes to the low-amplitude ambient signals in the 1- to 10-Hz range arriving at backazimuths between 280° and 320°.

The high sample rate also results in recording numerous high-frequency (>10 Hz) ambient infrasound and sub-bass signals, which appear as repetitive signals from relatively stable backazimuths, consistent with local anthropogenic sources. We do not attempt to identify the various local infrasound sources, but major clusters in derived backazimuths between ∼160 and 260° of signals >5 Hz are consistent with nearby towns including Atlimeyaya and Atlixco, possibly representing signals from traffic, industrial activity, power plants, airplanes, fireworks, etc. Diurnal variation of these detections is complicated, indicating combined effects of diurnal variations in source activity, atmospheric propagation conditions, variations in site noise conditions, and competition and interference between different sources in the same frequency band (Matoza et al., 2019). Identification of local infrasound sources could be achieved in future by deploying more infrasound arrays and using backazimuth cross-bearings to localize the sources (e.g., Matoza et al., 2017). Popocatépetl is surrounded by numerous villages and towns, highlighting the need for multiple infrasound arrays at different azimuths around the volcano for robust source discrimination in a future monitoring context.

3.2. Automated Explosion Signal Detection

Vulcanian explosions during the study period at Popocatépetl produced high-amplitude and rapid-onset infrasound at ATLI (Figure 3), signal features which can be exploited for automated detection. PMCC-derived amplitudes are higher than for any other signals recorded by ATLI during this time (Figure 2 symbol size), providing a simple criterion for automated detection (high-amplitude, coherent signal, originating from direction of Popocatépetl). We also separately apply a network-coincident STA/LTA (short-term average/long-term average) detector to the four ATLI infrasound channels (Beyreuther et al., 2010; Withers et al., 1998). We use a recursive STA/LTA method with an STA length of 0.5 s, an LTA length of 40 s, and triggering with an STA/LTA threshold ratio of 30 on at least three channels, a high value appropriate for high-amplitude explosion signals (Matoza et al., 2014). This produces six STA/LTA triggers, five of which coincide with the high-amplitude PMCC arrivals originating from the direction of Popocatépetl (Figure 2) and that we manually verify as explosion signals (Figure 3 and supporting information Figures S2–S6); the sixth results from a nonphysical data glitch. We subsequently focus on these five high-amplitude explosion events. A summary of information in the Centro Nacional de Prevención de Desastres (CENAPRED) observatory reports for the five Popocatépetl explosions considered in this study is provided in the supporting information, Table S1.

Lower STA/LTA thresholds of 20 and 10 increase the numbers of triggers to 20 and 196, respectively. Manual inspection reveals that the 14 additional triggers resulting from lowering the STA/LTA threshold from 30 to 20 are not signals from Popocatépetl and may be signals from local anthropogenic sources (e.g., con-

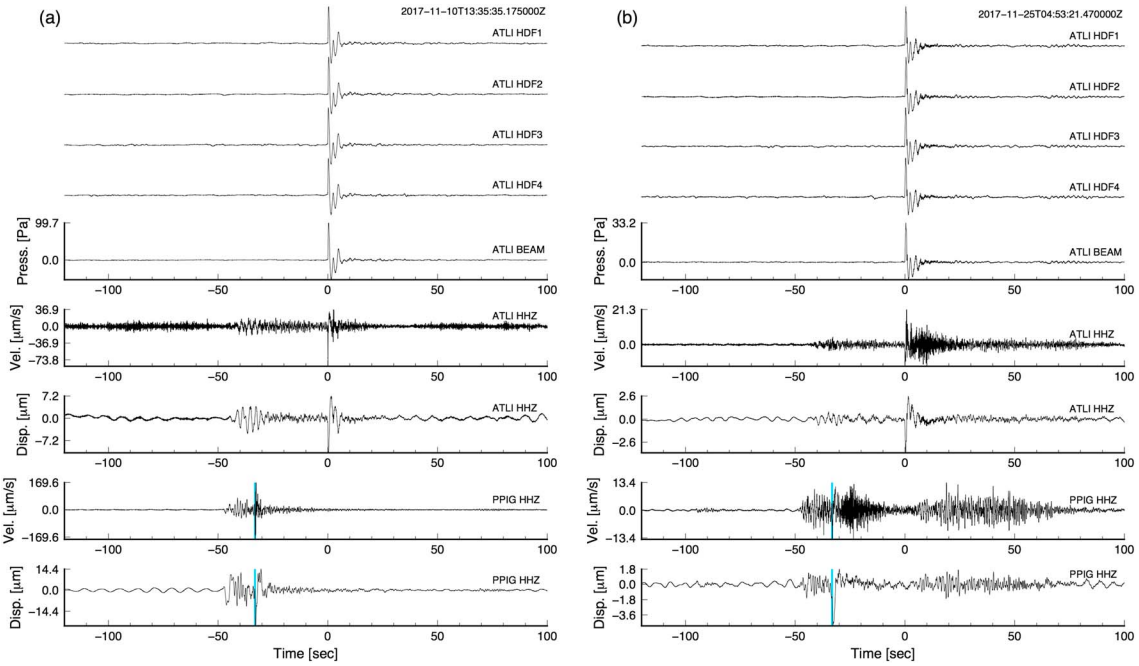

Figure 3. (a) Waveforms for a Popocatépetl explosion signal arriving at ATLI at 13:35:35.175 10 November (day 314) 2017; all times in UT. Zero time for all displayed waveforms corresponds to the network-coincident STA/LTA trigger time at ATLI (13:35:35.175 10 November 2017). We show waveforms for stations ATLI and PPIG. Channel labels HDF1–HDF4 correspond to the four channels of the ATLI infrasound array and BEAM to the traces aligned for the backazimuth of Popocatépetl (283.7°) and a trace velocity of 350 m/s derived from PMCC. Channel label HHZ refers to the vertical seismic component. Axis labels indicate physical units of pressure, velocity, or displacement in each case. The vertical blue bars on PPIG waveforms indicate the estimated arrival time of the airwave at PPIG given the difference in source-receiver distance (airwave arrives 33.2 s earlier at PPIG than ATLI) assuming a propagation velocity of 330 m/s. All waveforms shown are unfiltered, except for a high-pass filter above 0.01 Hz applied in deriving the displacement waveforms. (b) Same as Figure 3a, but for a Popocatépetl explosion signal arriving at ATLI at 04:53:21.470 25 November (day 329) 2017; all times in UT. Compared to the event shown in Figure 3a, this event has a lower acoustic amplitude and a more complex seismic wave train. The infrasound records help with identifying the air-ground-coupled arrival at PPIG and recognizing its contribution to the recorded seismic waveform. STA/LTA = short-term average/long-term average.

struction), lightning strikes, or nonphysical data glitches, confirming that the STA/LTA threshold of 30 is appropriate. It is possible that the data contain additional lower-amplitude or nonimpulsive signals (e.g., tremor) from Popocatépetl, which we do not attempt to identify here. The high level of ambient anthropogenic noise presents additional challenges to infrasound signal identification and discrimination, beyond the scope considered here.

4. Seismoacoustic Signature of Vulcanian Explosions

We focus on the five high-amplitude explosion events identified in Section 3. Two of these events are shown here in Figure 3, while similar plots for the remaining three events are included as supporting information (Figures S2–S6). All waveforms shown in Figure 3 are unfiltered, with the exception that a high-pass filter above 0.01 Hz was applied in deriving the displacement waveforms prior to integrating the velocity records. All instrument responses have been removed.

The highest amplitude event of the five is shown in Figure 3a (peak pressure of 99.7 Pa at ATLI), while Figure 3b shows a lower-amplitude event (peak pressure of 33.2 Pa at ATLI) with a more complex seismic wave train. Although the observed infrasound amplitudes vary from ~30 to 100 Pa, the infrasound waveform signatures for all five events are consistent and highly correlated. Utilizing a waveform sample from −5 to 50 s around the trigger time, the beamed infrasound data for the different explosions are all correlated with one another with maximum correlation coefficients above 0.91. That is except for the 24 November (day 328) event, which has maximum correlation coefficients of ~0.6–0.74 with the other events, likely resulting from additional noise contaminating this recording (see supporting information, Figures S7–S11). The high correlation between different events indicates that the explosion mechanism itself is repetitive; we interpret this as infrasound

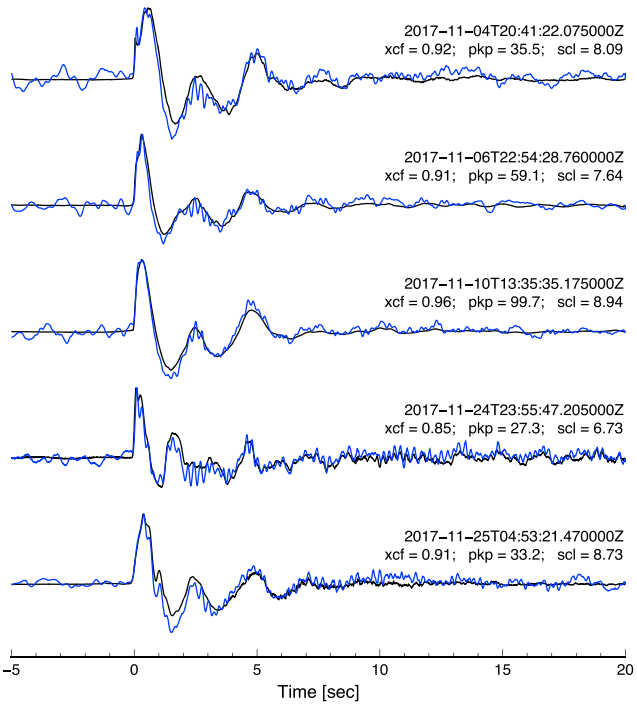

Figure 4. Comparison of infrasonic pressure waveforms (black) with inverted vertical displacement waveforms (blue) for the five large explosion events as recorded at ATLI. The infrasonic waveforms are beamformed traces with unit gain. The displacement waveforms are inverted by multiplying the original displacement trace by −1. The small relative time shift has been removed based on beamforming equations for the azimuth of Popocatépetl and acoustic trace velocity observed with PMCC (350 m/s). For each event we label `xcf`: the maximum correlation coefficient between infrasound beam and inverted displacement waveform; `pkp`: the peak pressure [Pa] of the infrasound waveform; and `scl`: the amplitude scale factor [Pa/μm] needed to scale the inverted displacement waveform with the pressure trace, based on matching peak pressure and peak inverted displacement.

waveforms dominated by a rapid pressure release, with minor waveform differences arising from additional source complexity and variety in fragmentation.

The seismic waveforms for each explosion share common features, with sustained seismic phases arriving prior to a ground-coupled airwave (air-ground converted wave) (e.g., De Angelis et al., 2012; Fee et al., 2016; Garces et al., 2000; Petersen & McNutt, 2007), which is delayed consistent with differences in seismic and infrasonic propagation velocities. The air-ground-coupled arrival is clearly visible in the vertical velocity waveforms, and the methods of Ichihara et al. (2012) and Matoza and Fee (2014) produce characteristic cross-correlation and coherence signatures between infrasound pressure and seismic vertical velocity waveforms (see supporting information, Figures S12–S16).

Additionally, here we find that inverted vertical displacement waveforms track the infrasonic pressure waveforms well and consistently for all five explosions (Figure 4). In Figure 4, we have artificially polarity-reversed the displacement waveform by multiplying the original displacement trace by −1, corresponding to a 180° phase shift. We also scale the inverted displacement waveforms to the pressure waveforms based on the waveform maxima (values of `scl` ranging from 6.73 to 8.94 Pa/μm, Figure 4). In addition, we have removed the delay time resulting from acoustic wave propagation between the seismic and infrasound sensors using beamforming equations (e.g., DeFatta et al., 1988) to simulate a colocated seismoacoustic sensor pair.

Inverted vertical seismic displacement and acoustic pressure waveforms are highly correlated, with normalized correlation coefficients of 0.85–0.96 (Figure 4) obtained using the full waveform duration from −5 to 20 s shown in Figure 4 (i.e., pressure and vertical displacement are anticorrelated). The derived amplitude-scale factors of ~7–9 Pa/μm are based simply on the waveform maxima but are relatively consistent for all five explosions. We do not attempt quantitative modeling of the pressure and displacement waveforms (Ichihara et al., 2012; Sabatier et al., 1986; Tanimoto & Wang, 2018), but presumably the amplitude-scale factor is related to the elastic properties of the near-surface material in which the seismometer is buried, in particular, the impedance. To first order, a positive pressure change at the ground surface pushes down on the ground, resulting in a downward vertical displacement, while a pressure decrease (negative pressure change) at the surface results in an upward vertical displacement. Similar vertical displacement signatures are observed at PPIG at the predicted airwave arrival time (Figure 3). A similar observation was noted by Yamada et al. (2016) for Vulcanian explosions at Lokon-Empung volcano, Indonesia, with a downward displacement phase excited by an infrasonic explosion wave arrival. In addition, de Groot-Hedlin et al. (2008) showed an *N*-wave signal from the shuttle Atlantis with a similar relationship between infrasonic pressure and vertical displacement waveforms, but with a more complex seismic waveform.

For the event shown in Figure 3b, the air-ground-coupled arrival in the ATLI vertical seismic velocity waveform has an additional broadband coda component, which is apparent in the infrasound waveform and presumably results from additional source complexity (e.g., Johnson et al., 2009; Matoza et al., 2014; Yamada et al., 2016). An arrival with similar waveform features appears in the PPIG data at the predicted airwave arrival time.

The relatively high sample rate (200 Hz) allows us to examine the spectral signature of Popocatépetl's Vulcanian explosions and associated air-ground coupling up to the Nyquist frequency of 100 Hz (Figure 5). The power spectral density estimates of the infrasound explosion waveforms (Figures 5a and 5e) reveal that these signals are not limited to the infrasound range (<20 Hz) but extend throughout the sub-bass range, remaining above noise up to the 100-Hz upper limit of our data. Such wave arrivals would likely be perceived by humans as an audible very low frequency sound, and/or felt. The constant slope of the spectrum from the

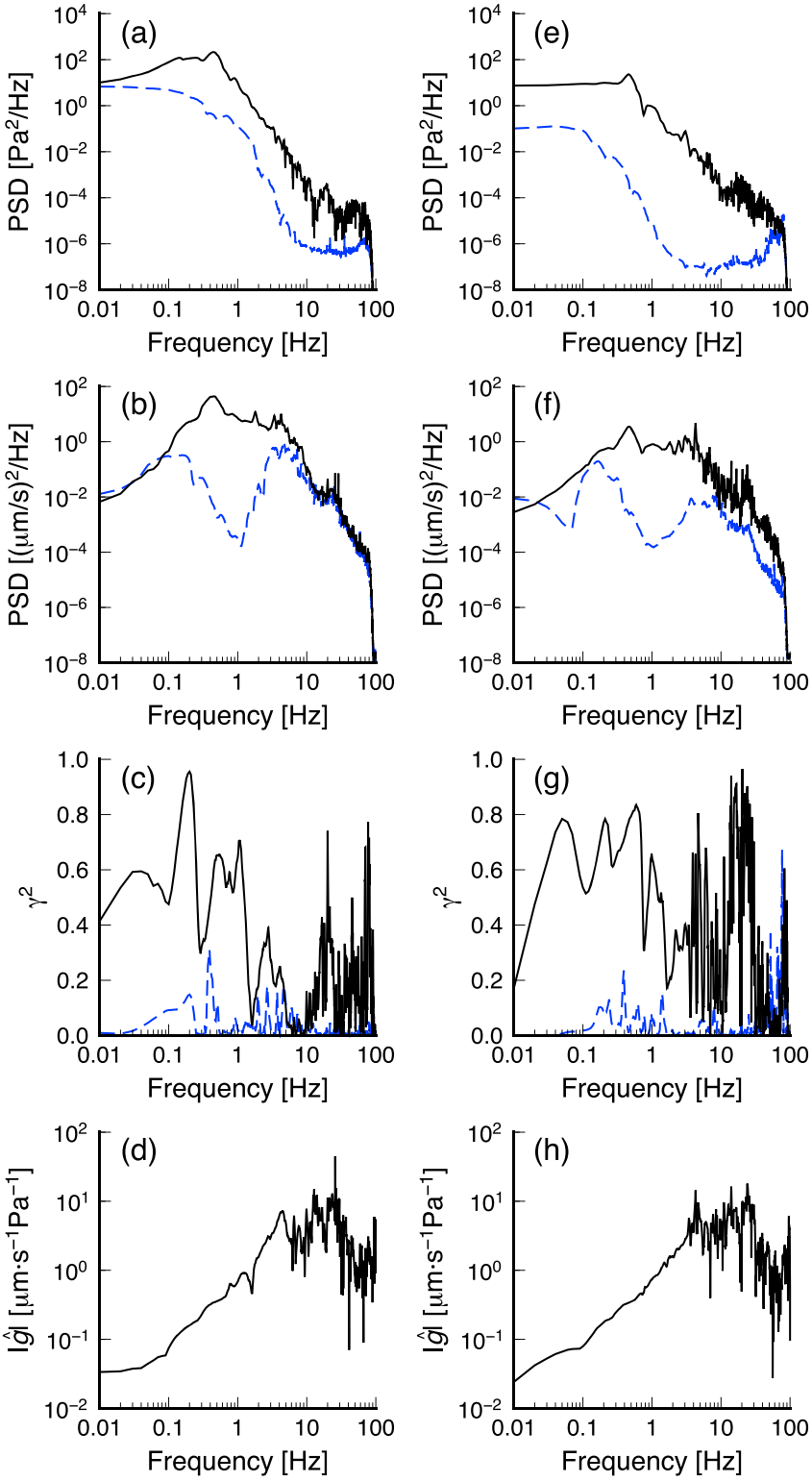

Figure 5. Seismoacoustic cross-spectral analysis for Figures 5a–5d: 13:35:35.175 10 November (day 314) 2017 event (shown in Figure 3a) and Figures 5e–5h: 04:53:21.470 25 November (day 329) 2017 event (shown in Figure 3b). (Figures 5a and 5e) Power spectral density of infrasonic waveform; (Figures 5b and 5f) power spectral density of vertical seismic velocity waveform; (Figures 5c and 5g) coherence; and (Figures 5d and 5h) gain of the transfer function. Black lines are for the signal from −50 to 50 s around the trigger time. Blue dashed lines are for a 100-s noise sample prior to the trigger.

peak frequency near 0.5 Hz up to 100 Hz indicates a common source process for this wide frequency content, and a seamless transition between the infrasound and sub-bass frequency ranges, likely involving nonlinear source and propagation effects to some degree (Atchley, 2005; Ishihara, 1985; Marchetti et al., 2013; Matoza et al., 2019; Yokoo & Ishihara, 2007). Above about 10 Hz, however, we observe additional bumps in the spectra which we attribute to additional source complexity (see spectrogram figures, supporting information, Figures S7–S11). The coherence analysis (Figure 5) similarly indicates air-ground coupling across this wide frequency range ~0.01–100 Hz, but observation above 10 Hz is limited by the noise levels in the seismic data. We note the increase in gain of the transfer function as a function of frequency (Figures 5d and 5h), which has previously been observed and attributed to a site response dependent upon near-surface geology (Matoza & Fee, 2014).

Station PPIG was formerly named PPM and seismic velocity waveforms recorded at this location associated with Popocatépetl explosions are presented in the study by Arciniega-Ceballos et al. (1999). Comparison of waveform amplitudes between the present study and those of Arciniega-Ceballos et al. (1999) and Chouet et al. (2005) indicate that the explosions analyzed in this study have magnitudes similar to past explosions.

Our results reaffirm the utility of infrasound data in interpreting seismic waveforms recorded at volcanoes. Specifically, our results indicate that air-ground-coupled infrasound contributes significantly to seismic waveforms associated with Vulcanian explosions at Popocatépetl. Our results also suggest that vertical seismic displacement waveforms may be exploited to identify and characterize high-amplitude infrasound explosion waveforms, even in the absence of dedicated infrasound data.

5. Conclusions

We observe clear seismoacoustic waveform signatures of five Vulcanian explosions at Popocatépetl volcano, Mexico, in November 2017 using a high-broadband infrasound array. For each explosion, we observe a high-amplitude and rapid-onset infrasound waveform that is air-ground coupled, with inverted vertical displacement waveforms tracking infrasonic pressure waveforms. Infrasound data facilitate the interpretation of seismic data at volcanoes, allowing significant air-ground-coupled arrivals to be identified in seismic waveforms. Infrasound technology has clear potential to augment the existing monitoring systems at Popocatépetl; however, high levels of anthropogenic noise are observed. Ambient anthropogenic infrasound source distributions should be considered in the design of future infrasound monitoring networks at populated volcanoes.

Acknowledgments
This work was supported by a grant from the University of California Institute for Mexico and the United States (UC MEXUS) and the Consejo Nacional de Ciencia y Tecnología de Mexico (CONACYT). Additional support provided by NSF grant EAR-1620576 and Universidad Nacional Autónoma de México project number DGAPA PAPIIT IN105617. G. M. P. and A. R. F. acknowledge scholarships from CONACYT. We thank Escuela Secundaria Publica in San Baltazar Atlimeyaya, Puebla, Mexico, especially the director teacher Elia F. China Torres and her group for the generous permission to install and operate the ATLI station on school grounds. Figure 1 basemap GeoTIFF NASA Earth Observatory image created by Jesse Allen using EO-1 ALI data. Figure 1 contours use NASA's Advanced Spaceborne Thermal Emission and Reflection Radiometer (ASTER) global DEM downloaded with GeoMapApp. Station PPIG data were obtained by the Servicio Sismológico Nacional (SSN), Universidad Nacional Autónoma de México (SSN, 2017); station maintenance, data acquisition, and distribution are made possible by SSN personnel. Our analysis included the use of ObsPy (Beyreuther et al., 2010; Krischer et al., 2015) and PMCC (Le Pichon et al., 2010), and we used Generic Mapping Tools (GMT) for plotting (Wessel & Smith, 1991). We thank Oliver Lamb and an anonymous reviewer for their comments that helped improve the paper. Waveform data are available in the supporting information.

References

Ahern, T. K., & Dost, B. (2012). SEED standard for the exchange of earthquake data reference manual format version 2.4. Incorporated Research Institutions for Seismology (IRIS). Retrieved from http://www.fdsn.org/seed_manual/SEEDManual_V2.4.pdf

Arámbula-Mendoza, R., Valdés-González, C., Varley, N., Juárez-García, B., Alonso-Rivera, P., & Hernández-Joffre, V. (2013). Observation of Vulcanian explosions with seismic and acoustic data at Popocatépetl volcano, Mexico. In V. M. Zobin (Ed.), *Complex monitoring of volcanic activity: Methods and results* (pp. 13–33). New York: Nova.

Arámbula-Mendoza, R., Valdés-González, C., Varley, N., Reyes-Pimentel, T. A., & Juárez-García, B. (2016). Tremor and its duration-amplitude distribution at Popocatépetl volcano, Mexico. *Geophysical Research Letters*, *43*, 8994–9001. https://doi.org/10.1002/2016GL070227

Arciniega-Ceballos, A., Chouet, B. A., & Dawson, P. (1999). Very long-period signals associated with vulcanian explosions at Popocatepetl volcano, mexico. *Geophysical Research Letters*, *26*(19), 3013–3016. https://doi.org/10.1029/1999GL005390

Arciniega-Ceballos, A., Chouet, B., & Dawson, P. (2003). Long-period events and tremor at Popocatepetl volcano (1994–2000) and their broadband characteristics. *Bulletin of Volcanology*, *65*(2-3), 124–135. https://doi.org/10.1007/s00445-002-0248-8

Arciniega-Ceballos, A., Chouet, B., Dawson, P., & Asch, G. (2008). Broadband seismic measurements of degassing activity associated with lava effusion at Popocatépetl volcano, Mexico. *Journal of Volcanology and Geothermal Research*, *170*(1–2), 12–23. https://doi.org/10.1016/j.jvolgeores.2007.09.007

Arciniega-Ceballos, A., Dawson, P., & Chouet, B. A. (2012). Long period seismic source characterization at Popocatépetl volcano, Mexico. *Geophysical Research Letters*, *39*, L20307. https://doi.org/10.1029/2012GL053494

Arciniega-Ceballos, A., Valdes Gonzalez, C., & Dawson, P. (2000). Temporal and spectral characteristics of seismicity observed at Popocatepetl volcano, central Mexico. *Journal of Volcanology and Geothermal Research*, *102*(3–4), 207–216. https://doi.org/10.1016/S0377-0273(00)00188-8

Atchley, A. A. (2005). Not your ordinary sound experience: A nonlinear-acoustics primer. *Acoustics Today*, *1*(1), 19–24.

Beyreuther, M., Barsch, R., Krischer, L., Megies, T., Behr, Y., & Wassermann, J. (2010). ObsPy: A Python toolbox for seismology. *Seismological Research Letters*, *81*(3), 530–533. https://doi.org/10.1785/gssrl.81.3.530

Cansi, Y. (1995). An automatic seismic event processing for detection and location: The P.M.C.C. method. *Geophysical Research Letters*, *22*(9), 1021–1024.

Cansi, Y., & Klinger, Y. (1997). An automated data processing method for mini-arrays. *Newsletter of the European-Mediterranean Seismological Centre*, *11*, 2–4.

Chouet, B., Dawson, P., & Arciniega-Ceballos, A. (2005). Source mechanism of vulcanian degassing at Popocatepetl volcano, Mexico, determined from waveform inversions of very long period signals. *Journal of Geophysical Research*, *110*, B070301. https://doi.org/10.1029/2004JB003524

Coffin, M. F., Gahagan, L. M., & Lawver, L. A. (1998). Present-day plate boundary digital data compilation. University of Texas Institute for Geophysics Technical Report 174.
De Angelis, S., Fee, D., Haney, M., & Schneider, D. (2012). Detecting hidden volcanic explosions from Mt. Cleveland volcano, Alaska with infrasound and ground-coupled airwaves. *Geophysical Research Letters*, *39*, L21312. https://doi.org/10.1029/2012GL053635
de Groot-Hedlin, C. D., Hedlin, M. A. H., Walker, K. T., Drob, D. P., & Zumberge, M. A. (2008). Evaluation of infrasound signals from the shuttle Atlantis using a large seismic network. *Journal of the Acoustical Society of America*, *124*(3), 1442–1451. https://doi.org/10.1121/1.2956475
De la Cruz-Reyna, S., Quezada, J. L., Peña, C., Zepeda, O., & Sánchez, T. (1995). Historia de la actividad reciente del Popocatépetl (1354–1995). In C. Científico Asesor CENAPRED-UNAM (Ed.), *Volcán Popocatépetl: Estudios realizados durante la crisis de 1994–1995* (pp. 3–22). Mexico City
De la Cruz-Reyna, S., & Siebe, C. (1997). The giant Popocatépetl stirs. *Nature*, *388*, 227. https://doi.org/10.1038/40749
De la Cruz-Reyna, S., Yokoyama, I., Martínez-Bringas, A., & Ramos, E. (2008). Precursory seismicity of the 1994 eruption of Popocatépetl volcano, central Mexico. *Bulletin of Volcanology*, *70*(6), 753–767. https://doi.org/10.1007/s00445-008-0195-0
DeFatta, D. J., Lucas, J. G., & Hodgkiss, W. S. (1988). *Digital signal processing: A system design approach*. New York: John Wiley.
Delgado-Granados, H., De la Cruz-Reyna, S., & Tilling, R. I. (2008). The 1994–present eruption of Popocatépetl volcano: Background, current activity, and impacts. *Journal of Volcanology and Geothermal Research*, *170*(1-2), 1–4. https://doi.org/10.1016/j.jvolgeores.2007.09.003
Fee, D., Haney, M., Matoza, R., Szuberla, C., Lyons, J., & Waythomas, C. (2016). Seismic envelope-based detection and location of ground-coupled airwaves from volcanoes in Alaska. *Bulletin of the Seismological Society of America*, *106*(3). https://doi.org/10.1785/0120150244
Fee, D., & Matoza, R. S. (2013). An overview of volcano infrasound: From Hawaiian to Plinian, local to global. *Journal of Volcanology and Geothermal Research*, *249*, 123–139. https://doi.org/10.1016/j.jvolgeores.2012.09.002
Garcés, M. A., Fee, D., & Matoza, R. S. (2013). Volcano acoustics. In S. A. Fagents, T. K. P. Gregg, & R. M. C. Lopes (Eds.), *Modeling volcanic processes* (Vol. 16, pp. 359–383). California: Cambridge University Press.
Garcés, M., Harris, A., Hetzer, C., Johnson, J., Rowland, S., Marchetti, E., & Okubo, P. (2003). Infrasonic tremor observed at Kilauea volcano, Hawaii. *Geophysical Research Letters*, *30*(20), 2023. https://doi.org/10.1029/2003GL018038
Garces, M. A., McNutt, S. R., Hansen, R. A., & Eichelberger, J. C. (2000). Application of wave-theoretical seismoacoustic models to the interpretation of explosion and eruption tremor signals radiated by Pavlof volcano, Alaska. *Journal of Geophysical Research*, *105*(B2), 3039–3058. https://doi.org/10.1029/1999JB900096
Global Volcanism Program (2013). Volcanoes of the world. In E. Venzke (Ed.), *Smithsonian Institution*. Washington, DC. 4.5.3, Downloaded 6 Nov 2014 https://doi.org/10.5479/si.GVP.VOTW4-2013
Ichihara, M., Takeo, M., Yokoo, A., Oikawa, J., & Ohminato, T. (2012). Monitoring volcanic activity using correlation patterns between infrasound and ground motion. *Geophysical Research Letters*, *39*, L04304. https://doi.org/10.1029/2011GL050542
Ishihara, K. (1985). Dynamical analysis of volcanic explosion. *Journal of Geodynamics*, *3*(3-4), 327–349. https://doi.org/10.1016/0264-3707(85)90041-9
Johnson, J. B., & Ripepe, M. (2011). Volcano infrasound: A review. *Journal of Volcanology and Geothermal Research*, *206*(3-4), 61–69. https://doi.org/10.1016/j.jvolgeores.2011.06.006
Johnson, J. B., Sanderson, R., Lyons, J., Escobar-Wolf, R., Waite, G., & Lees, J. M. (2009). Dissection of a composite volcanic earthquake at Santiaguito, Guatemala. *Geophysical Research Letters*, *36*, L16308. https://doi.org/10.1029/2009GL039370
Krischer, L., Megies, T., Barsch, R., Beyreuther, M., Lecocq, T., Caudron, C., & Wassermann, J. (2015). ObsPy: A bridge for seismology into the scientific Python ecosystem. *Computational Science & Discovery*, *8*(1), 014003. https://doi.org/10.1088/1749-4699/8/1/014003
Landès, M., Ceranna, L., Le Pichon, A., & Matoza, R. S. (2012). Localization of microbarom sources using the IMS infrasound network. *Journal of Geophysical Research*, *117*, D06102. https://doi.org/10.1029/2011JD016684
Le Pichon, A., Matoza, R., Brachet, N., & Cansi, Y. (2010). Recent enhancements of the PMCC infrasound signal detector. *Inframatics, September 2010*, *26*, 5–8.
Marchetti, E., Ripepe, M., Delle Donne, D., Genco, R., Finizola, A., & Garaebiti, E. (2013). Blast waves from violent explosive activity at Yasur volcano, Vanuatu. *Geophysical Research Letters*, *40*, 5838–5843. https://doi.org/10.1002/2013GL057900
Martin Del Pozzo, A. L., Alatorre Ibargüengoitia, M., Arana Salinas, L., Bonasia, R., Capra Pedol, L., Cassata, W., et al. (2017). Estudios geológicos y actualización del mapa de peligros del volcán Popocatépetl: Memoria técnica del mapa de peligros del volcán. *Monografías del Instituto de Geofísica, Universidad Nacional Autónoma de México*.
Matoza, R. S., & Fee, D. (2014). Infrasonic component of volcano-seismic eruption tremor. *Geophysical Research Letters*, *41*, 1964–1970. https://doi.org/10.1002/2014GL059301
Matoza, R., Fee, D., Green, D., & Mialle, P. (2019). Volcano infrasound and the International Monitoring System. In A. Le Pichon, E. Blanc, & A. Hauchecorne (Eds.), *Infrasound monitoring for atmospheric studies: Challenges in middle-atmosphere dynamics and societal benefits* (Vol. 33, pp. 1023–1077). Cham: Springer. https://doi.org/10.1007/978-3-319-75140-5_33
Matoza, R. S., Fee, D., & López, T. M. (2014). Acoustic characterization of explosion complexity at Sakurajima, Karymsky, and Tungurahua volcanoes. *Seismological Research Letters*, *85*(6), 1187–1199. https://doi.org/10.1785/0220140110
Matoza, R. S., Green, D. N., Le Pichon, A., Shearer, P. M., Fee, D., Mialle, P., & Ceranna, L. (2017). Automated detection and cataloging of global explosive volcanism using the International Monitoring System infrasound network. *Journal of Geophysical Research: Solid Earth*, *122*, 2946–2971. https://doi.org/10.1002/2016JB013356
Matoza, R. S., Hedlin, M. A. H., & Garcés, M. A. (2007). An infrasound array study of Mount St. Helens. *Journal of Volcanology and Geothermal Research*, *160*(3-4), 249–262. https://doi.org/10.1016/j.jvolgeores.2006.10.006
Matoza, R. S., Landès, M., Le Pichon, A., Ceranna, L., & Brown, D. (2013). Coherent ambient infrasound recorded by the International Monitoring System. *Geophysical Research Letters*, *40*, 429–433. https://doi.org/10.1029/2012GL054329
Panfil, M. S., Gardner, T. W., & Hirth, K. G. (1999). Late Holocene stratigraphy of the Tetimpa archaeological sites, northeast flank of Popocatépetl volcano, central Mexico. *GSA Bulletin*, *111*(2), 204–218. https://doi.org/10.1130/0016-7606(1999)111<0204:LHSOTT>2.3.CO;2
Petersen, T., & McNutt, S. R. (2007). Seismo-acoustic signals associated with degassing explosions recorded at Shishaldin volcano, Alaska, 2003–2004. *Bulletin of Volcanology*, *69*(5), 527–536. https://doi.org/10.1007/s00445-006-0088-z
Raga, A. C., Raga, G. B., Cantó, J., & Alfonso, L. (2002). Atmospheric expansion wave simulations of Popocatepetl explosions. *Journal of Geophysical Research*, *107*(D16), 4304. https://doi.org/10.1029/2001JD000693
Roman, D. C. (2017). Automated detection and characterization of harmonic tremor in continuous seismic data. *Geophysical Research Letters*, *44*, 6065–6073. https://doi.org/10.1002/2017GL073715
SSN (2017). Servicio sismológico nacional, instituto de geofísica, Universidad Nacional Autónoma de México, México. Retrieved from http://www.ssn.unam.mxhttps://doi.org/10.1029/2012GL054329

Sabatier, J. M., Bass, H. E., Bolen, L. N., & Attenborough, K. (1986). Acoustically induced seismic waves. *Journal of the Acoustical Society of America*, *80*, 646649. https://doi.org/10.1121/1.394058

Siebe, C., Abrams, M., & Macías, J. L. (1995). Derrumbes gigantes, depósitos de avalancha de escombros y edad del actual cono del volcán Popocatépetl. In C. Científico Asesor CENAPRED-UNAM (Ed.), *Volcán Popocatépetl: Estudios realizados durante la crisis de 1994–1995*, (pp. 195–220).

Siebe, C., Abrams, M., Macías, J. L., & Obenholzner, J. (1996). Repeated volcanic disasters in Prehispanic time at Popocatépetl, central Mexico: Past key to the future? *Geology*, *24*(5), 399–402. https://doi.org/10.1130/0091-7613(1996)024<0399:RVDIPT>2.3.CO;2

Siebe, C., Schaaf, P., & Urrutia-Fucugauchi, J. (1999). Mammoth bones embedded in a late Pleistocene lahar from Popocatépetl volcano, near Tocuila, central Mexico. *GSA Bulletin*, *111*(10), 1550–1562. https://doi.org/10.1130/0016-7606(1999)111<1550:MBEIAL>2.3.CO;2

Tanimoto, T., & Wang, J. (2018). Low-frequency seismic noise characteristics from the analysis of co-located seismic and pressure data. *Journal of Geophysical Research: Solid Earth*, *123*, 5853–5885. https://doi.org/10.1029/2018JB015519

Walker, K. T., & Hedlin, M. A. H. (2010). A review of wind-noise reduction methodologies. In A. L. Pichon, E. Blanc, & A. Hauchecorne (Eds.), *Infrasound monitoring for atmospheric studies* (pp. 141–182). Netherlands: Springer.

Wessel, P., & Smith, W. H. F. (1991). Free software helps map and display data. *Eos, Transactions American Geophysical Union*, *72*(41), 441–446. https://doi.org/10.1029/90EO00319

Withers, M., Aster, R., Young, C., Beiriger, J., Harris, M., Moore, S., & Trujillo, J. (1998). A comparison of select trigger algorithms for automated global seismic phase and event detection. *Bulletin of the Seismological Society of America*, *88*(1), 95–106.

Yamada, T., Aoyama, H., Nishimura, T., Yakiwara, H., Nakamichi, H., Oikawa, J., et al. (2016). Initial phases of explosion earthquakes accompanying vulcanian eruptions at Lokon-Empung volcano, Indonesia. *Journal of Volcanology and Geothermal Research*, *327*, 310–321. https://doi.org/10.1016/j.jvolgeores.2016.08.011

Yokoo, A., & Ishihara, K. (2007). Analysis of pressure waves observed in Sakurajima eruption movies. *Earth Planet Space*, *59*(3), 177–181. https://doi.org/10.1186/BF03352691